Paper:

Pseudoinverse-Based Motion Control of a Redundant Manipulator on a Flexible Base with Vibration Suppression

Yusuke Fukazu, Naoyuki Hara, Toshimitu Hishinuma, Daisuke Sato*, and Yoshikazu Kanamiya**

Department of Mechanical Systems Engineering, Graduate School of Engineering, Musashi Institute of Technology
1-28-1 Tamazutsumi, Setagaya-ku, Tokyo 158-8557, Japan
E-mail: {*dsato, **nenchev}@sc.musashi-tech.ac.jp
[Received September 28, 2007; accepted December 10, 2007]

We propose a method for motion control of a redundant manipulator on a flexible base. Manipulator selfmotion is determined from a velocity-level additional constraint obtained from base vibration dynamics. End-effector path tracking is ensured via pseudoinverse-based velocity control. In this way, algorithmic singularities associated with the additional constraint are avoided. The vibration suppression control component is derived via the Singularity-Consistent method, which aleviates destabilization during vibration suppression in the vicinity of kinematic singularities. Experimental data from a 3R planar manipulator on a flexible base confirmed the feasibility of the proposed method.

Keywords: redundant manipulator, flexible-base manipulator, vibration suppression, singularity-consistent method, pseudoinverse matrix

1. Introduction

Many studies on flexible-base manipulators, or macro-mini manipulators[1], have focused on applications in space robotics (see e.g. [1]). We previously developed the *Reaction Null-Space* concept applied to motion planning and control of single-arm [2] and dual-arm [3] flexible-base manipulators. Based on this concept, we decomposed joint space to achieve dynamic decoupling between the macro and mini subsystems – suppressing vibration in the macro subsystem efficiently and generating reactionless motions. The reaction null-space concept was also applied to derive an adaptive vibration suppression control law [4].

Note, however, that in a single-arm manipulator, reactionless motion control implies that end-effector movement is confined to a specific path determined by the initial configuration. A few possible approaches to the problem have been proposed, based on *dynamic redundancy* and/or *kinematic redundancy* [2]. Dynamic redundancy was examined using the dual-arm flexible-base manipulator, with one arm operated as a manipulation (load-carrying) arm and the other was used solely to compensate for deflection in the flexible base. Unfortunately, the dual-arm scenario raises another problem: compensation maneuvers leading to unavoidable collisions between the two arms.

Using kinematic redundancy for simultaneous end-tip and base motion control has been proposed [5, 6] for free-flying space robots. A redundant mini manipulator was used in [7] to compensate for elastic deflections of a flexible-link macro subsystem.

The problem of end-effector motion control combined with vibration suppression was also addressed [8]. Vibration suppression control was derived from the manipulator Jacobian null space of the redundant mini subsystem. To avoid velocity build-up, multi-criteria were optimized, but this is computationally inefficient. We developed a control law for a flexible-base redundant manipulator based on the reaction null-space concept [9]. Although vibration was effectively suppressed, the imposed vibration suppression constraint lead to the appearance of *algorithmic singularities* located inside the workspace. It is not physically possible, however, to suppress vibration in such manipulator configurations [10].

Here we propose a control law combining effective vibration suppression control based on the Singularity-Consistent method [11], with pseudoinverse-based end-tip motion control that avoids algorithmic singularities.

This paper is organized as follows: Section 2 gives the background. Section 3 details the singularity-consistent solution to vibration suppression. Section 4 introduces Jacobian pseudoinverse-based modification of the main solution. Section 5 discusses experiments and implementation of the method. Section 6 presents experimental data and Section 7 lists conclusions.

2. Background

2.1. Reaction Null-Space Concept

The equation of motion of a manipulator on a flexible base with positional and orientational deflection $\Delta\boldsymbol{\xi} \in \Re^k$,

1. The macro manipulator plays the role of the flexible base.

is written as follows [2]:

$$\begin{bmatrix} \boldsymbol{H}_b(\Delta\boldsymbol{\xi},\boldsymbol{q}) & \boldsymbol{H}_{bm}(\Delta\boldsymbol{\xi},\boldsymbol{q}) \\ \boldsymbol{H}_{bm}^T(\Delta\boldsymbol{\xi},\boldsymbol{q}) & \boldsymbol{H}_m(\boldsymbol{q}) \end{bmatrix} \begin{bmatrix} \dot{\boldsymbol{\nu}}_b \\ \ddot{\boldsymbol{q}} \end{bmatrix} + \begin{bmatrix} \boldsymbol{D}_b\boldsymbol{\nu}_b \\ \boldsymbol{0} \end{bmatrix} + \begin{bmatrix} \boldsymbol{K}_b\Delta\boldsymbol{\xi} \\ \boldsymbol{0} \end{bmatrix} + \begin{bmatrix} \boldsymbol{c}_b(\Delta\boldsymbol{\xi},\boldsymbol{\nu}_b,\boldsymbol{q},\dot{\boldsymbol{q}}) \\ \boldsymbol{c}_m(\Delta\boldsymbol{\xi},\boldsymbol{\nu}_b,\boldsymbol{q},\dot{\boldsymbol{q}}) \end{bmatrix} = \begin{bmatrix} \boldsymbol{0} \\ \boldsymbol{\tau} \end{bmatrix} \quad (1)$$

where $\boldsymbol{\nu}_b \in \Re^k$ is the base twist, $\boldsymbol{q} \in \Re^n$ stands for the generalized coordinates of the arm, $\boldsymbol{H}_b$, $\boldsymbol{D}_b$, and $\boldsymbol{K}_b \in \Re^{k\times k}$ denote base inertia, damping and stiffness, $\boldsymbol{H}_m \in \Re^{n\times n}$ is the inertia matrix of the arm, $\boldsymbol{H}_{bm} \in \Re^{k\times n}$ stands for the *inertia coupling matrix*, $\boldsymbol{c}_b$ and $\boldsymbol{c}_m$ denote velocity-dependent nonlinear terms, and $\boldsymbol{\tau} \in \Re^n$ is joint torque. No external force acts either on the base or manipulator.

Under simplifying assumptions [2], the equation of motion is linearized around the base equilibrium, as follows:

$$\boldsymbol{H}_b\dot{\boldsymbol{\nu}}_b + \boldsymbol{D}_b\boldsymbol{\nu}_b + \boldsymbol{K}_b\Delta\boldsymbol{\xi} = -\boldsymbol{H}_{bm}\ddot{\boldsymbol{q}}. \quad (2)$$

Control acceleration is chosen as:

$$\ddot{\boldsymbol{q}} = \boldsymbol{H}_{bm}^+\boldsymbol{G}_b\boldsymbol{\nu}_b + (\boldsymbol{I} - \boldsymbol{H}_{bm}^+\boldsymbol{H}_{bm})\boldsymbol{\zeta}_A \quad (3)$$

where $\boldsymbol{G}_b$ is a positive definite constant matrix and $\boldsymbol{H}_{bm}^+ \in \Re^{n\times k}$ denotes the Moore-Penrose generalized inverse (pseudoinverse) of the inertia coupling matrix, $\boldsymbol{I}$ denotes the unit matrix of proper dimension, and $\boldsymbol{\zeta}_A$ is an arbitrary vector. Since $\boldsymbol{H}_{bm}\boldsymbol{H}_{bm}^+ = \boldsymbol{I}$ and $\boldsymbol{H}_{bm}(\boldsymbol{I} - \boldsymbol{H}_{bm}^+\boldsymbol{H}_{bm}) = \boldsymbol{0}$, damping is controlled by appropriately choosing matrix $\boldsymbol{G}_b$. Note that the second term on the RHS of the above equation stands for reaction null-space. The term was used to ensure the desired end-effector motion constraint [2].

The control law for vibration suppression can be adapted to manipulators driven under velocity control [2]. To do so, integrate Eq. (3) without the reaction null-space term to obtain:

$$\dot{\boldsymbol{q}} \approx \boldsymbol{H}_{bm}^+\boldsymbol{G}_b\Delta\boldsymbol{\xi}. \quad (4)$$

We assumed matrix $\boldsymbol{H}_{bm}^+$, a function of joint angles, to be constant. This is justified because base vibration dynamics are much faster than manipulator dynamics.

2.2. Redundancy Resolution Through Vibration Suppression Constraint

We developed control equations in terms of velocities because many joint-level controllers function in velocity control mode.

The imposed end-effector velocity constraint is as follows:

$$\boldsymbol{\nu}_e = \boldsymbol{J}(\boldsymbol{q})\dot{\boldsymbol{q}} \quad (5)$$

where $\boldsymbol{\nu}_e \in \Re^m$ denotes manipulator end-effector twist, and $\boldsymbol{J}(\boldsymbol{q}) \in \Re^{m\times n}$ is the manipulator Jacobian. This equation is underdetermined, and the set of solutions is expressed as:

$$\dot{\boldsymbol{q}} = \boldsymbol{J}^+(\boldsymbol{q})\boldsymbol{\nu}_e + (\boldsymbol{I} - \boldsymbol{J}^+(\boldsymbol{q})\boldsymbol{J}(\boldsymbol{q}))\boldsymbol{\zeta}_V \quad (6)$$

where $\boldsymbol{\zeta}_V$ denotes an arbitrary n-vector.

Unique joint velocity is determined from the above equation in different ways [12]. We impose an additional constraint, derived from the vibration suppression condition (4):

$$\boldsymbol{H}_{bm}\dot{\boldsymbol{q}} = \boldsymbol{G}_b\Delta\boldsymbol{\xi}. \quad (7)$$

Assume that dimension k of base deflection space equals the *degree of redundancy* of the manipulator, i.e., $k = n - m$. Combining the imposed end-effector velocity constraint (5) with the above additional constraint, we obtain:

$$\begin{bmatrix} \boldsymbol{\nu}_e \\ \boldsymbol{G}_b\Delta\boldsymbol{\xi} \end{bmatrix} = \boldsymbol{J}_{vs}\dot{\boldsymbol{q}} \quad (8)$$

where $\boldsymbol{J}_{vs} = \begin{bmatrix} \boldsymbol{J}^T & \boldsymbol{H}_{bm}^T \end{bmatrix}^T \in \Re^{n\times n}$. The unique joint velocity solution is then written as:

$$\dot{\boldsymbol{q}} = \boldsymbol{J}_{vs}^{-1} \begin{bmatrix} \boldsymbol{\nu}_e \\ \boldsymbol{G}_b\Delta\boldsymbol{\xi} \end{bmatrix}. \quad (9)$$

3. Singularity-Consistent Solution

Although the solution for the joint velocity vector was obtained straightforwardly, note that the system is destabilized if matrix $\boldsymbol{J}_{vs}$ becomes singular.

3.1. Algorithmic Singularity Analysis

Condition $\det\boldsymbol{J}_{vs} = 0$ means that the linear system (8) becomes singular. When displayed in workspace, singularities are mapped to both isolated points and continua. A well-known subclass of singularities is kinematic singularities, defined by condition $\det\boldsymbol{J}\boldsymbol{J}^T = 0$. For articulated manipulators, these appear mainly at workspace boundaries. Other singularities, called algorithmic singularities, are located within workspace, significantly hindering the task planning problem.

Example : Consider a 3-degree-of-freedom (DOF) planar manipulator on a flexible base (**Fig. 1**). The set of algorithmic singularities is graphically displayed within the workspace (**Fig. 2**). Curves are parameterized by the q_1 joint angle: the figure at left shows the set of algorithmic singularities for $q_1 = 0°$, and that at right – for $q_1 = 45°$.

The system destabilizes if the end-tip approaches a singularity curve.

3.2. Homogeneous Velocity Equation

To cope with the singularity problem, we rewrite the joint velocity solution based on the singularity-consistent method [11], representing the end-effector twist as:

$$\boldsymbol{\nu}_e = \dot{q}_*\boldsymbol{t}_* \quad (10)$$

where $\boldsymbol{t}_*$ is the normalized end-effector twist and $\dot{q}_*$ is twist magnitude. We compose a *column-augmented*

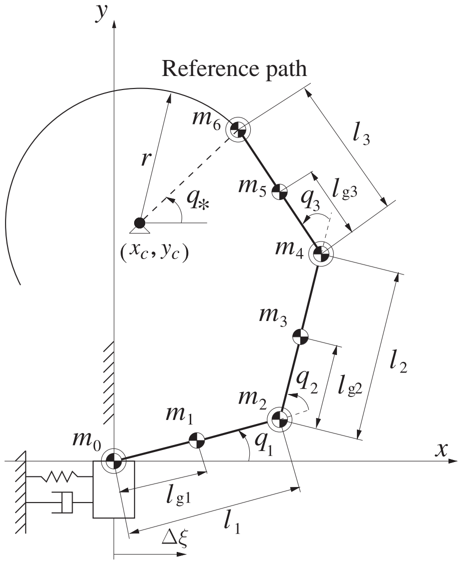

Fig. 1. Model of TREP-R.

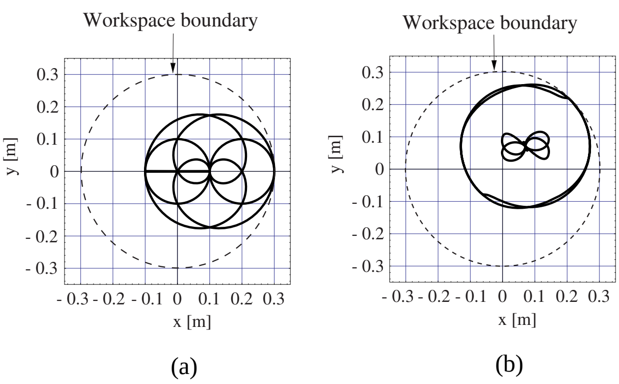

Fig. 2. Sets of algorithmic singularities in workspace: (a) $q_1 = 0°$, (b) $q_1 = 45°$.

Jacobian-based velocity equation as follows:

$$\bar{\boldsymbol{J}}_{vs}\bar{\dot{\boldsymbol{q}}} = \begin{bmatrix} \boldsymbol{J} & -\boldsymbol{t}_* & \boldsymbol{0} \\ \boldsymbol{H}_{bm} & \boldsymbol{0} & -\boldsymbol{G}_b\Delta\boldsymbol{\xi} \end{bmatrix} \begin{bmatrix} \dot{\boldsymbol{q}} \\ \dot{q}_* \\ 1 \end{bmatrix} = \boldsymbol{0}. \quad \text{(11)}$$

Column-augmented Jacobian matrix $\bar{\boldsymbol{J}}_{vs}$ is $n \times (n+2)$ and its kernel contains two nonzero vectors at nondegenerate configurations (full rank of $\bar{\boldsymbol{J}}_{vs}$). The set of solutions to the homogeneous equation is obtained as:

$$\bar{\dot{\boldsymbol{q}}} = b_m\bar{\boldsymbol{n}}_m + b_b\bar{\boldsymbol{n}}_b \quad \text{(12)}$$

where b_m and b_b are arbitrary scalars, and

$$\bar{\boldsymbol{n}}_m = \begin{bmatrix} \boldsymbol{n}_m^T & \det\boldsymbol{J}_{vs} & 0 \end{bmatrix}^T \in \Re^{n+2} \quad \text{(13)}$$

$$\bar{\boldsymbol{n}}_b = \begin{bmatrix} \boldsymbol{n}_b^T & 0 & \det\boldsymbol{J}_{vs} \end{bmatrix}^T \in \Re^{n+2} \quad \text{(14)}$$

are the two nonzero vectors in the kernel. Subscripts "m" and "b" denote components of the solution contributing to end-effector and to flexible base motion. Note that null-space vectors $\boldsymbol{n}_m$ and $\boldsymbol{n}_b$ are derived as null-space vectors of the two $n \times (n+1)$ minors of the column-augmented Jacobian. The minors are obtained by deleting the third and second columns of $\bar{\boldsymbol{J}}_{vs}$. Joint velocities in proportion to the $\boldsymbol{n}_m$ vector will keep the end-effector moving along twist $\boldsymbol{t}_*$ while satisfying constraint $\boldsymbol{H}_{bm}\dot{\boldsymbol{q}} = \boldsymbol{0}$. This means that the above joint velocities belong to the reaction null-space. Note that joint velocities proportional to the $\boldsymbol{n}_b$ vector are selfmotion joint velocities that satisfy the vibration suppression constraint.

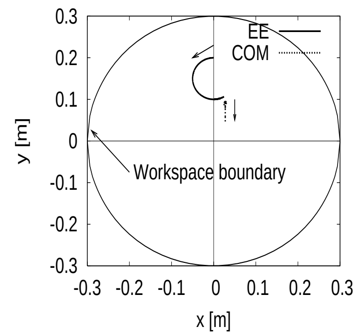

Fig. 3. CoM restriction along y axis.

The last solution is expanded as follows:

$$\dot{\boldsymbol{q}} = b_m\boldsymbol{n}_m + b_b\boldsymbol{n}_b \quad \text{(15)}$$

$$\dot{q}_* = b_m \det\boldsymbol{J}_{vs} \quad \text{(16)}$$

$$1 = b_b \det\boldsymbol{J}_{vs}. \quad \text{(17)}$$

If b_m and b_b are determined from the last two equations and substituted into Eq. (15), the joint velocity obtained will be the same as that in Eq. (9), and the system may destabilize around singularities.

One way to deal with this problem is by appropriately choosing arbitrary scalars b_m and b_b – the essence of the singularity-consistent method. We sacrifice performance in end-effector speed along the desired path and in vibration suppression, but gain overall stability.

Note an important property of the above solution: the $b_m\boldsymbol{n}_m$ component restricts manipulator motion conservatively due to the reaction null-space constraint. Algorithmic singularities appear as a consequence of this constraint. In our 3-DOF manipulator, the reaction null-space constraint restricts CoM to moving only in the direction of y, while the end-tip tracks the reference circular arc (see **Fig. 3**). This is not desirable because an algorithmic singularity will inevitably be reached [9].

4. Pseudoinverse-Based Solution

To relax the constraint on CoM motion, we use a Moore-Penrose generalized inverse (pseudoinverse) based velocity component for end-effector motion. To do this, replace $b_m\boldsymbol{n}_m$ in Eq. (15) with the Jacobian pseudoinverse-based solution for inverse kinematics:

$$\dot{\boldsymbol{q}} = \boldsymbol{J}^+(\boldsymbol{q})\boldsymbol{\nu}_e + b_b\boldsymbol{n}_b. \quad \text{(18)}$$

When analyzing the above equation, note that the set of joint velocities $\dot{\boldsymbol{q}}_n = b_b\boldsymbol{n}_b$ satisfies the two constraints:

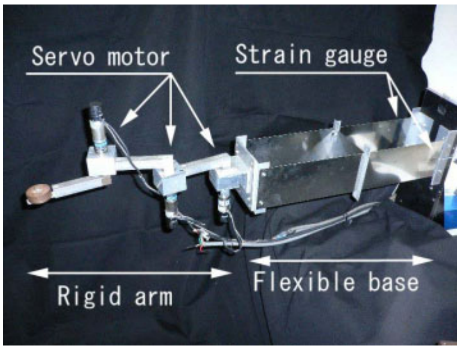

Fig. 4. TREP-R experimental setup.

Table 1. Manipulator link parameters.

l_1, l_2, l_3	0.1 m
l_{g1}, l_{g2}, l_{g3}	0.05 m
m_1, m_3, m_5	0.025 kg
m_2, m_4	0.285 kg
m_6	0.095 kg

$\boldsymbol{J}(\boldsymbol{q})\dot{\boldsymbol{q}}_n = \boldsymbol{0}$ and $\boldsymbol{H}_{bm}\dot{\boldsymbol{q}}_n = \boldsymbol{G}_b\Delta\boldsymbol{\xi}$. The first constraint means that vector $\boldsymbol{n}_b$ belongs to the null space of the Jacobian: $\boldsymbol{n}_b \in \mathscr{N}(\boldsymbol{J})$. From the pseudoinverse-based inverse kinematics solution for kinematically redundant manipulators, it is concluded that the two components of joint velocity are orthogonal [12]. Their mutual interference is thus minimized, and we expect that the vibration suppression constraint will be enforced constantly during end-effector motion but without disturbing it.

5. Experimental System

Our experimental setup, TREP-R (**Fig. 4**) is planar, consisting of a 3R rigid arm manipulator attached to the free end of an elastic double beam representing the flexible base. Due to the design, we assume that the base deflects only longitudinally, so the reaction moment and the reaction force component along the transverse axis of the base can be neglected as a disturbance. The deflection of the flexible base is measured by a strain gauge. Manipulator motor controllers operate in velocity control mode.

5.1. Dynamic TREP-R model

In the system model (**Fig. 1**) arm and base parameters are shown in **Tables 1** and **2**. The natural angular frequency, damping ratio, and base stiffness were estimated using the logarithmic decrement applied to damped free vibration experimental data. Natural angular frequency is 12.66 rad/s and the damping ratio is 0.011. Note that the reference path is designed as a circular arc of radius r, centered at (x_c, y_c). The end-tip twist magnitude is represented by the rate of change of arc angle $\dot{q}_*$.

Table 2. Flexible base parameters.

Length	0.4 m
Height	0.1 m
Width	0.09 m
Thickness	1×10^{-3} m
Tip mass $h_b (\equiv m_0)$	0.45 kg
Stiffness k_b	191 N/m
Damping d_b	0.33 Ns/m

5.2. TREP-R velocity control

There is one degree of redundancy because the manipulator has 3-DOF ($n = 3$) and we control the positioning of the end-tip ($m = 2$). This means that $k = 1$. As stated, only longitudinal base deflection is considered. Matrix $\boldsymbol{J}_{vs}$ is 3×3. The additional constraint for vibration suppression, as in Eq. (7), becomes:

$$\boldsymbol{h}_{bm}\dot{\boldsymbol{q}} = g_b\Delta\xi. \quad (19)$$

Note that because we consider one-DOF base deflection, gain g_b and base deflection $\Delta\xi$ are expressed as scalar values. Inertia coupling matrix $\boldsymbol{h}_{bm}$ is represented as a 1×3 row-matrix. The column-augmented Jacobian matrix from Eq. (8) is written as:

$$\bar{\boldsymbol{J}}_{vs} = \begin{bmatrix} \boldsymbol{J} & -\hat{\boldsymbol{v}} & 0 \\ \boldsymbol{h}_{bm} & 0 & -g_b\Delta\xi \end{bmatrix} \in \Re^{3\times 5} \quad (20)$$

where $\boldsymbol{v}$ denotes the end-tip velocity vector. The “hat” stands for a unit vector (i.e., end-tip velocity direction in this case).

The null-space vector for vibration suppression calculated from column-augmented matrix $\bar{\boldsymbol{J}}_{vs}$ can be written as $\boldsymbol{n}_b = g_b\Delta\xi\tilde{\boldsymbol{n}}_b(\boldsymbol{q})$. The three components of vector $\tilde{\boldsymbol{n}}_b(\boldsymbol{q})$ are:

$$\begin{aligned} \tilde{n}_{b1} &= l_2 l_3 \sin q_3 \\ \tilde{n}_{b2} &= -l_3(l_2 \sin q_3 + l_1 \sin(q_2 + q_3)) \\ \tilde{n}_{b3} &= l_1(l_2 \sin q_2 + l_3 \sin(q_2 + q_3)). \end{aligned} \quad (21)$$

For manipulator end-tip control, we use the pseudoinverse of the manipulator Jacobian, as mentioned. Thus, from Eq. (18) we obtain:

$$\dot{\boldsymbol{q}} = \boldsymbol{J}^+(\boldsymbol{q})\boldsymbol{v}_{ref} + b_b\boldsymbol{n}_b \quad (22)$$

as the control equation. $\boldsymbol{v}_{ref}$ is the reference end-tip velocity, calculated under the following feedback control law:

$$\boldsymbol{v}_{ref} = \boldsymbol{v} + \boldsymbol{K}(\boldsymbol{p}_d - \boldsymbol{p}). \quad (23)$$

$\boldsymbol{v} \equiv \dot{\boldsymbol{p}}_d = \dot{q}_*\hat{\boldsymbol{v}}$ is the desired end-tip velocity, and $\boldsymbol{p}_d$ and $\boldsymbol{p}$ are desired and actual end-tip positions. The actual end-tip position is obtained through forward kinematics based on data for joint angles $\boldsymbol{q}$ and base deflection $\Delta\xi$. Note that base deflection is needed for null-space vector $\boldsymbol{n}_b$ in Eq. (22). $\boldsymbol{K}$ is a positive-definite feedback gain matrix. The TREP-R control block diagram is shown in **Fig. 5**.

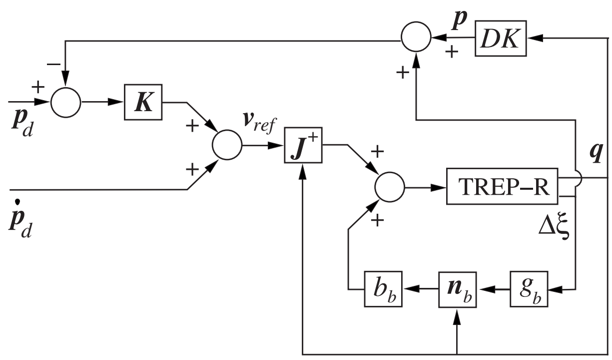

Fig. 5. Control block diagram.

6. Experiments

In our two experiments, the end-tip should track a full circle of radius 0.08 m for 6 seconds, starting with initial configuration $\boldsymbol{q} = [139°, -53°, -60°]^T$. Feedback gain matrix $\boldsymbol{K}$ is a diagonal matrix, and both elements are set to $10\ \mathrm{s}^{-1}$. The sampling time interval is set to 1 ms.

In the first experiment, scalar b_b was set to zero, i.e., no vibration suppression invoked, so results (**Fig. 6**) show the path tracking performance under pseudoinverse control alone. The base deflection graph shows that, initially, only slight vibrations were induced. When the end-tip passed close to the kinematic singularity, confirmed from the kinematic singularity (KS) determinant graph (i.e., the graph displays $\det \boldsymbol{J}\boldsymbol{J}^T$), large vibrations were induced. These vibrations were not suppressed, as expected.

In the second simulation, vibration suppression was enabled via a nonzero b_b. Best performance is achievable when b_b is derived from Eq. (17). Here, however, b_b was set to a nonzero constant, $b_b = 2\ \mathrm{m}^{-3}\mathrm{s}^{-1}$, to avoid destabilization around the kinematic singularity. The vibration suppression gain was set at $g_b = 10\ \mathrm{s}^{-1}$.

The base deflection graph shows that the base deflects significantly near the kinematic singularity, as in the first experiment, but thereafter vibrations are suppressed (**Fig. 7**). The system does not destabilize, despite crossing the algorithmic singularity (AS determinant graph, showing that $\det \boldsymbol{J}_{vs}$ changes sign at 2 ms).

7. Conclusions

We have shown that kinematic redundancy is helpful in reducing vibration in flexible-base manipulators. The end-tip of the manipulator tracks the reference path while redundancy is being resolved through an additional constraint derived from base vibration dynamics. We focused here on algorithmic singularities induced by the additional constraint. We concluded that the center of mass motion should not be restricted conservatively, and showed this is achieved using the pseudoinverse, to ensure also proper end-tip motion control.

Unfortunately, end-tip path tracking under pseudoinverse control destabilizes the system, inducing large vi-

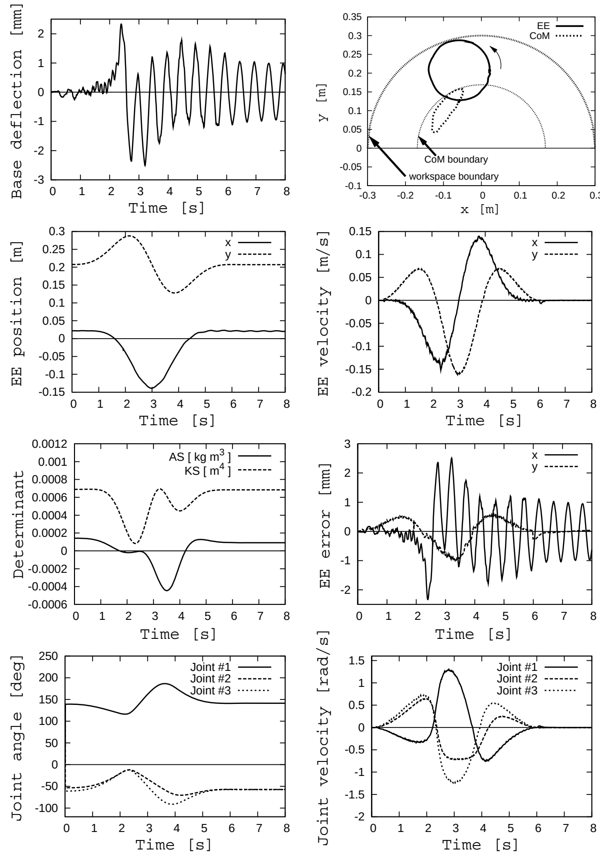

Fig. 6. Circular path tracking without vibration suppression.

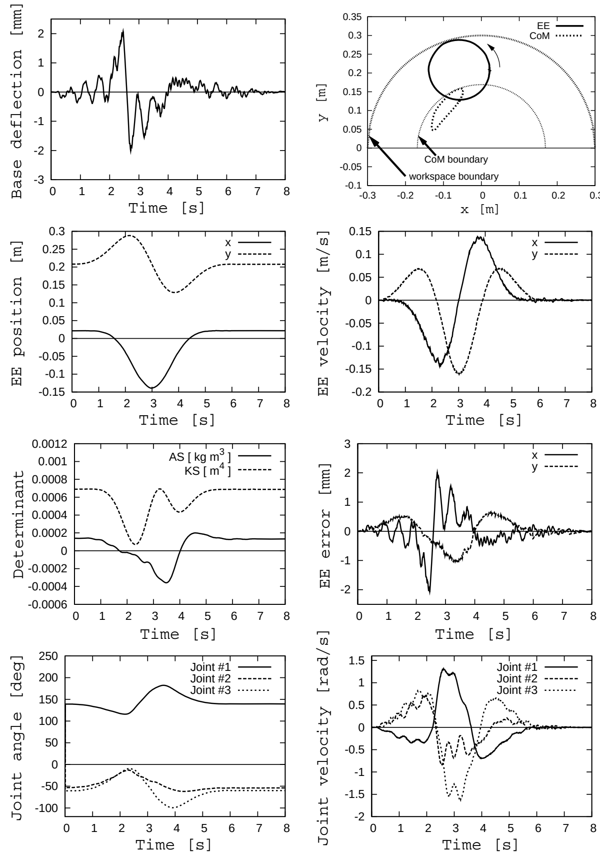

Fig. 7. Circular path tracking with vibration suppression.

brations around kinematic singularities. We suppressed these large vibrations by using a vibration suppression joint velocity component, derived via the singularity-consistent method.

References:

[1] M. A. Torres and S. Dubowsky, "Path-planning in elastically constrained space manipulator systems," Proc. IEEE Int. Conf. Robotics and Automation, Atlanta, Georgia, pp. 812-817, 1993.

[2] D. N. Nenchev et al., "Reaction Null-Space control of flexible structure mounted manipulator systems," IEEE Tr. on Robotics and Automation, Vol.15, No.6, pp. 1011-1023, December, 1999.

[3] A. Gouo et al., "Motion control of dual-arm long-reach manipulators," Advanced Robotics, Vol. 13, No. 6, pp. 617–632, 2000.

[4] S. Abiko and K. Yoshida, "An Adaptive Control of a Space Manipulator for Vibration Suppression," 2005 IEEE/RSJ Int. Conf. on Intelligent Robots and Systems, Edmonton, pp. 2167-2172, Canada, August 2-August 6, 2005.

[5] D. N. Nenchev, K. Yoshida, and Y. Umetani, "Introduction of redundant arms for manipulation in space," IEEE Int. Workshop on Intelligent Robots and Systems, pp. 679-684, Tokyo, Japan, 1988.

[6] R. D. Quinn, J. L. Chen, and C. Lawrence, "Redundant manipulators for momentum compensation in microgravity environment," Proc. AIAA Guidance, Navigation and Control Conf., pp. 581-587, New York, 1988.

[7] T. Yoshikawa et al., "Quasi-static trajectory tracking control of flexible manipulator by macro-micro manipulator system," Proc. IEEE Int. Conf. Robotics and Automation, Vol.3, pp. 210-214, Atlanta, May 1993.

[8] M. Hanson and R. Tolson, "Reducing flexible base vibrations through local redundancy resolution," Journal of Robotic Systems, Vol.12, No.11, pp. 767-779, 1995.

[9] T. Hishinuma and D. N. Nenchev, "Singularity-Consistent Vibration Suppression Control With a Redundant Manipulator Mounted on a Flexible Base," 2006 IEEE/RSJ Int. Conf. on Intelligent Robots and Systems, pp. 3237-3242, Beijing, China, October 9-October 15, 2006.

[10] L. E. George and W. J. Book, "Inertial vibration damping control of a flexible-base manipulator," IEEE/ASME Tr. on Mechatronics, Vol.8, No.2, pp. 268-271, June, 2003.

[11] D. N. Nenchev, Y. Tsumaki, and M. Uchiyama, "Singularity-consistent parameterization of robot motion and control," The International Journal of Robotics Research, Vol.19, No.2, pp. 159-182, February, 2000.

[12] D. N. Nenchev, "Redundancy resolution through local optimization: a review," Journal of Robotic Systems, Vol. 6, No. 6, pp. 769-798, 1989.

Name:
Yusuke Fukazu

Affiliation:
Master Student, Department of Mechanical Systems Engineering, Faculty of Engineering, Musashi Institute of Technology

Address:
1-28-1 Tamazutsumi, Setagaya-ku, Tokyo 158-8557, Japan

Brief Biographical History:
2003- Student, Musashi Institute of Technology
2007- Student, Graduate School of Musashi Institute of Technology

Name:
Naoyuki Hara

Affiliation:
Master Student, Department of Mechanical Systems Engineering, Faculty of Engineering, Musashi Institute of Technology

Address:
1-28-1 Tamazutsumi, Setagaya-ku, Tokyo 158-8557, Japan

Brief Biographical History:
2004- Student, Musashi Institute of Technology
2008- Student, Graduate School of Musashi Institute of Technology

Name:
Toshimitsu Hishinuma

Affiliation:
Equipment group, Jyukuukan material division, Dai Nippon Printing Co., Ltd.

Address:
642-8 Mitsuugaki, Okayama, Okayama 709-2121, Japan

Brief Biographical History:
2007 Joined Dai Nippon Printing Co., Ltd.

Main Works:
• T. Hishinuma and D. N. Nenchev, "Singularity-Consistent Vibration Suppression Control With a Redundant Manipulator Mounted on a Flexible Base," 2006 IEEE/RSJ Int. Conf. on Intelligent Robots and Systems, pp. 3237-3242, Beijing, China, October 9-October 15, 2006.

Name:
Daisuke Sato

Affiliation:
Lecturer, Department of Mechanical Systems Engineering, Faculty of Engineering, Musashi Institute of Technology

Address:
1-28-1 Tamazutsumi, Setagaya-ku, Tokyo 158-8557, Japan

Brief Biographical History:
2000- JSPS Research Fellowships for Young Scientists
2002- Research Associate, Tohoku University
2007- Lecturer, Musashi Institute of Technology

Main Works:
• "Soft Tissue Pushing Operation Using a Haptic Interface for Simulation of Brain Tumor Resection," Journal of Robotics and Mechatronics, Vol.18, No.5, pp. 634-642, 2006.
• "Dexterous Motion Design for a DD Parallel Robot," Robotics Research, The Eleventh International Symposium, Springer Tracts in Advanced Robotics, Vol.15, pp. 26-35, 2005.

Membership in Academic Societies:
• The Japan Society of Mechanical Engineers (JSME)
• The Robotics Society of Japan (RSJ)
• The Society of Instrument and Control Engineering of Japan (SICE)
• The Institute of Electrical and Electronics Engineers (IEEE)

Name:
Yoshikazu Kanamiya (D. N. Nenchev)

Affiliation:
Professor, Department of Mechanical Systems Engineering, Faculty of Engineering, Musashi Institute of Technology

Address:
1-28-1 Tamazutsumi, Setagaya-ku, Tokyo 158-8557, Japan

Brief Biographical History:
1985- Technical University of Sofia
1994- Tohoku University
1997- Niigata University
1999- Hirosaki University
2003- Musashi Institute of Technology

Main Works:
• "Analysis of a redundant free-flying spacecraft/manipulator system," IEEE Transactions on Robotics and Automation, Vol.8, No.1, pp. 1-6, January 1992.

Membership in Academic Societies:
• The Japan Society of Mechanical Engineers (JSME)
• The Robotics Society of Japan (RSJ)
• The Society of Instrument and Control Engineering of Japan (SICE)
• The Institute of Electrical and Electronics Engineers (IEEE)